Journal of Microelectronics and Electronic Packaging (2013) **10**, 129-137
Copyright © International Microelectronics Assembly and Packaging Society
ISSN: 1551-4897

Tin Nanoparticle-Based Solder Paste for Low Temperature Processing

Alfredo J. Diaz,[1] David Ma,[2] Alfred Zinn,[2] and Pedro O. Quintero[1,*]

***Abstract*—Materials have shown a tendency to modify their bulk properties depending on powder particle size. Nanoparticles' coalescence temperature tends to decrease as particle size decreases. Taking advantage of this behavior, a nanoparticle-based solder paste has been developed as a proof-of-concept and is described in this paper for attaching electronic components at a lower processing temperature to avoid thermally induced damage and reduce energy consumption.**

Tin nanoparticles were successfully synthesized via a wet chemistry route. The synthesis consists on the use tin (II) chloride dehydrated as the Sn precursor, 1,10-phenanthroline as the surfactant, and sodium borohydride as the reducing agent. A flux system was developed based on ethylene glycol. The solder paste based on the synthesized Sn nanoparticles showed good surface wetting, but not a sufficient metal volume to produce an attachment because the paste required high flux content, thus resulting in a poor metallic load paste. By using commercially procured Sn nanoparticles the results showed acceptable coalescence of the noncapped nanoparticles at temperatures as low as 200°C with a processing time of 20 min. A reduction in processing temperature of approximately 40°C has been found when comparing the developed solder paste with typical SAC lead-free solders. The mechanical and electrical properties of the resulting structure were characterized by means of lap-shear testing and a four-wire Kelvin test showing acceptable shear strength and electrical conductivity.

***Keywords*—Nanosolder, tin nanoparticles, lead-free, solder, solder paste, sintering, melting point depression, shear strength, electrical conductivity**

Introduction

The semiconductor industry generates more than $298 billion annually according to the Semiconductor Industry Association [1]. Most of the revenue is from the sales of consumer electronics, that is, cellphones, laptops, tablets, and so on. This industry has encountered technical difficulties after legislation, called the Restriction of Hazardous Substances (RoHS), banned the use of some materials, mainly lead (Pb), that have been used for many years; thus resulting in manufacturing and reliability problems with the integration of new technologies. The major impacts of lead-free soldering in electronics can be attributed to higher soldering temperatures and the increased complexity of the microstructures of solder joints. The main issue is that higher soldering temperatures might cause damage to temperature-sensitive components [2].

The peak reflow or processing temperature of Pb-free alloys will increase, for example, from 220°C when using conventional Sn-37Pb eutectic solder to ~250°C when using a Sn-Ag-Cu alloy, causing potential damage to electronic components that cannot withstand such high reflow temperatures [3]. As part of this investigation, mechanisms that reduce the coalescence temperature of the particles, such as melting point depression or sintering, will be investigated in order to produce an attachment at a temperature below the bulk melting point.

Melting point depression of nanoparticles is an intrinsic property where the decrease in particle size is poised to significantly reduce the melting point of the material due to the increase of surface energy [4-8] (this is well established both experimentally and theoretically [9]). The graph in Fig. 1 shows the significant decrease in melting point with particle size for tin.

Sintering is a thermal treatment for bonding particles into a coherent, predominantly solid structure via mass transport events that often occur at the atomic scale. The bonding leads to improved strength and lower system energy [10]. The temperature needed to induce bonding through sintering depends on material and particle size. Most materials exhibit sintering behavior between temperatures around 0.5-0.8 T_m (bulk). Bonds and densification become more evident with higher temperatures, longer times, and smaller particles [11].

A solder paste is a homogeneous and kinetically stable mixture of solder alloy powder (Sn nanoparticles, in this case), flux, and vehicle, which is capable of forming metallurgical bonds at a given soldering condition [12] and that have the properties required by the manufacturing process. After reflow, the solder will have a bulk behavior. The reflow process will induce nanoparticles to coalesce. The consolidation of the nanoparticles will increase the particle or cluster size, thus reducing the total surface energy of the system. The advantage of this process will be to have a higher melting temperature of the solder at application conditions than in processing due to densification of the metal content, hence annihilating the effect of size-dependency on the melting point.

Many researchers have reported the thermal characteristics of nanoparticles accounting for a reduction in the melting point. Schmidt et al. [13] published that they have found irregular variations in the melting point of size-selected clusters. Using calorimetric analysis developed by Lai et al. [5] for

Received on July 26, 2013; revision received on September 17, 2013; accepted on September 22, 2013
[1]Department of Mechanical Engineering, University of Puerto Rico-Mayaguez
[2]Lockheed Martin Corporation
This work was supported by Lockheed Martin Corporation.
*Corresponding author; email: pedro.quintero@upr.edu

doi:10.4071/imaps.386 1551-4897 © 2013 International Microelectronics Assembly and Packaging Society

Downloaded from http://meridian.allenpress.com/jmep/article-pdf/10/4/129/2244967/imaps_386.pdf by guest on 31 October 2022

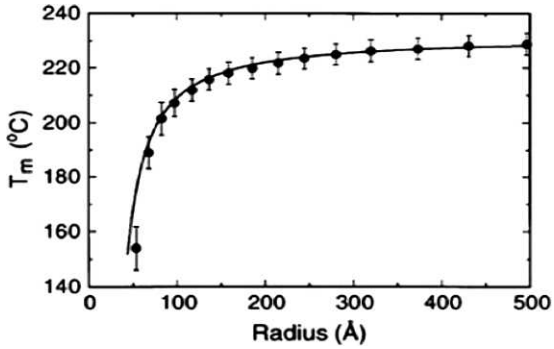

Fig. 1. Melting point size dependence of tin nanoparticles. The solid line is based on theory and the point are experimental results [5].

isolated tin nanoparticles, they experimentally acquired data for clusters of different sizes finding irregular tendencies, thus concluding that the size dependence of the melting point cannot be explained easily and depends on a complicated interplay between geometric and electronic structure. Jiang et al. [14], in 2007, published work based on synthesis and thermal characterization of Sn-Ag alloy particles. They synthesized the nanoparticles using a low temperature wet chemistry route with a surfactant to reduce the agglomeration and oxidation of the nanoparticles. For an average particle size of 10 nm, differential scanning calorimetry (DSC) revealed a melting point of around 194°C. Zou et al. [6] published that tin nanoparticles, synthesized via a wet chemistry route, resulted in diameters of 81, 40, 36, and 34 nm that had a melting points of 226.1, 221.8, 221.1, and 219.5°C, respectively, according to DSC measurements.

Taking advantage of the lower coalescence temperature found for nanoparticles, some researchers have used this to produce nanosolder paste for lower processing temperatures. Hsiao et al. [15] published their findings on the properties of a solder based on SAC chemically synthesized nanoparticles mixed with a Rosin mildly activated commercial flux (TACFLUX®, Indium Corp.) to produce a paste. The processing temperature of the solder paste was reduced to almost 215°C and they reported favorable wetting of the surface. Liu et al. [16] concluded in their review paper that pure nanosolder pastes are a relatively new research subject and it should be studied down to its core to take advantage of the lower melting point. Jiang et al. [8] synthesized tin, tin/silver (SnAg), and tin/silver/copper (SnAgCu) alloy nanoparticles of various sizes to prepare a solder paste. They developed a flux based on citric acid and ethanol having a low reflow temperature. The wetting test for the as-prepared SnAg and SnAgCu alloy nanoparticle pastes on a Cu surface showed the typical Cu_6Sn_5 intermetallic compound (IMC) formation.

Methodology

A. Synthesis of Sn Nanoparticles

The experimental setup used to control the parameters of the synthesis is shown in Fig. 2. The reaction chamber was isolated from ambient conditions; argon was used to minimize the presence of air in the chamber where the reactor is a jacketed beaker connected to a Thermo Scientific Neslab RTE7 chiller to control the temperature at which the reaction occurs. A magnetic stirrer was used for the homogenization of the solution.

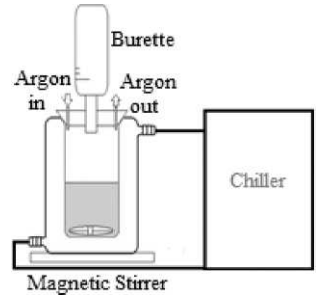

Fig. 2. Schematic of synthesis setup.

An aqueous solution of 100 mL 0.1 M $SnCl_2 \cdot 2H_2O$ was prepared in glyme (1,2 dimethoxyethane) and 2 g of 1,10-phenanthroline were added to the solution (for a 1:1 molar ratio of phen:$SnCl_2$). The solution was then added to the reaction chamber and magnetically stirred for 10 min at a controlled temperature of 20°C. A 100 mL suspension of 1.5 g sodium borohydride in glyme was then added to the reaction chamber and held for 1 h. The resulting solution was then centrifuged at 9,000 RPM for 5 min, and then redispersed in ethanol for cleaning. This process was repeated three times, and the samples were then vacuum dried. All the chemicals were supplied by Sigma-Aldrich®. The resulting material was analyzed using XRD and TEM.

B. Development of Flux and Solder Paste

The flux was developed and tested by formulating a solder paste consisting of commercially procured Sn microparticles (1-5 μm). Samples of the paste were reflowed at 250°C to ensure the fusion of the metallic particles. The behavior of the flux was assessed qualitatively for each experimental combination in order to find the best formulation. The flux constituents are ethylene glycol and glutamic acid, mixed into specific experimental ratios, ranging from 5-50 wt.% concentrations, for screening purposes. Different flux compositions were mixed with a metallic particulate in order to find the optimal embodiment of the paste. The specific quantities of each constituent of the solder paste were weighted, mixed, and homogenized for the preparation.

C. Experimental Sample Preparation

The preparation of the samples consisted of the use of a Cu foil as a test coupon. The solder paste containing the Sn nanoparticles was deposited on top of the substrate by using the process of stencil printing (0.1 mm in thickness). Different experimental thermal profiles were used to process the samples after which the coalescence of the nanoparticles was characterized. After processing, the samples were cleaned using acetone and sonication for 10 min. SEM and EDS was used to characterize the resulting material.

D. Lap Shear Testing

Lap shear tests were performed in order to characterize the mechanical strength of the joints at different test conditions of time and processing temperatures. Two Cu foil strips were cut to 2 in. long, and then a stencil (0.014 in. thickness) was used

Downloaded from http://meridian.allenpress.com/jmep/article-pdf/10/4/129/2244967/imaps_386.pdf by guest on 31 October 2022

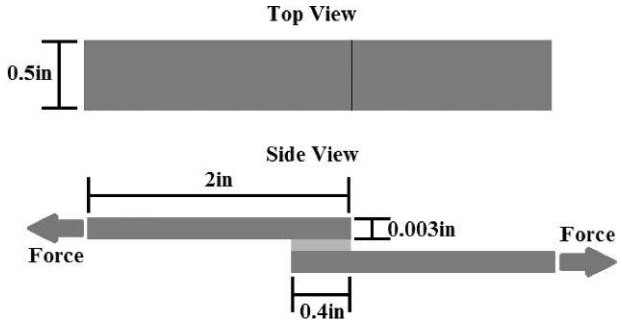

Fig. 3. Lap shear test specimen schematic.

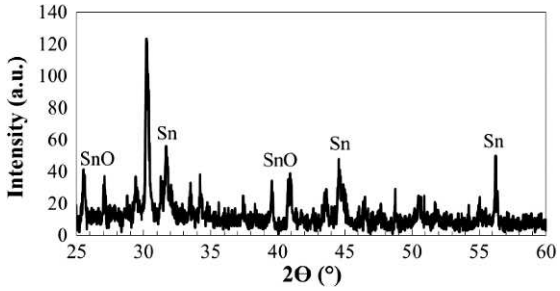

Fig. 4. XRD pattern for the synthesized nanoparticles.

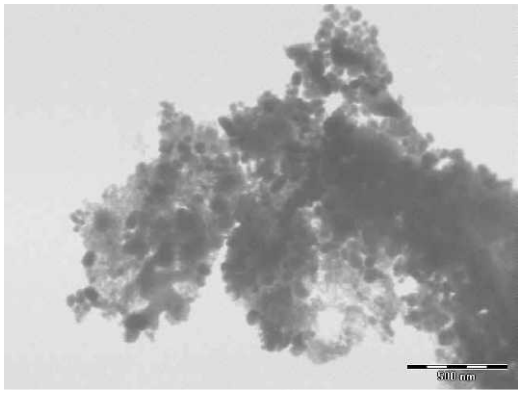

Fig. 5. TEM image for the synthesized Sn nanoparticles.

to print a square of solder paste in the tip of one strip with a length of 0.4 in., as shown in Fig. 3.

The mechanical testing equipment used was a Mark 10-ESM301L®. The reported shear strength is the average of 10 samples for each testing condition.

E. Electrical Properties Testing

The electrical conductivity of the sintered tin nanoparticles was measured and compared with the bulk value reported in literature. The electrical resistance of the material was measured using a Digital Milli-ohm meter (model 310 of BK precision) based on a four wire Kelvin test. The four wire Kelvin test working principle is to supply a current between two points and measure the voltage drop across two points, maintaining a constant distance between the probes across all the samples measured. The material's electrical resistivity was calculated based on the measured resistance and geometrical parameters. Samples were prepared using the obtained optimal processing parameters using a glass substrate to measure the resistivity of the metallic material. The electrical conductivity was calculated as the average of 15 samples per condition (ambient or argon atmosphere during processing).

F. Differential Scanning Calorimetry

Thermal analysis was performed on the nanoparticles for the understanding of the coalescence mechanism. The instrument used was a DSC-e by Instrument Specialists®. The analysis of the Sn nanoparticles was conducted in an inert atmosphere (argon flowing at 15 cc/min) where samples were heated at a ramp rate of 10°C/min up to a peak temperature of 250°C. Different ramp rates and peak temperatures were used to analyze the behavior of the flux when heated in reflow-like thermal profiles. Off-line thermogravimetry was used to estimate the quantity of material left in the solder after the thermal profiles.

Results and Discussion

A. Synthesized Sn Nanoparticles

X-ray diffraction (XRD) was used to characterize the synthesized material. Fig. 4 shows the XRD pattern for the dried residues from the synthesis. The intensity peaks showed a mixture of tin and tin oxide (as identified by the Match! software standard library); further, NaCl was detected as a product of the reaction. Fig. 5 shows a TEM image for the synthesized Sn nanoparticles. Particle sizes of 30-60 nm in diameter were recovered from our synthesis.

The flux formulation was aimed at improving the oxide removal capability from the surface of the particles. Ethylene glycol was mixed with glutamic acid (from 5-50 wt.% concentration) to use as the flux medium. A solder paste was developed by adding quantities ranging from 85-95 wt.% metallic tin microparticles and tested at a reflow temperature of 250°C. Qualitative observations were used to select the best flux formulation to later produce the Sn nanoparticle solder paste.

From the set of experimental trials, the best paste composition was selected for performing tests with the synthesized Sn nanoparticles. Using the particles from the synthesis, a solder paste was developed using the most effective flux combination obtained from the preliminary tests with Sn microparticles. The nanosolder paste formulation was a mixture of the driedproduct from the synthesis with the flux using a ratio of 25 wt.% nanoparticles and 75 wt.% flux (50 wt.% of ethylene glycol and 50 wt.% of glutamic acid). Due to the small particle size, more flux was needed in the mixture to produce a solder paste with the appropriate rheology. Rheological properties were assessed by qualitative means such as printability. Further quantitative tests, as for example viscosity measurements, will be a focus of future work.

Reflow was performed on copper test coupons where the solder paste was deposited on top. Temperatures ranging from 195°C to 220°C were used to process the samples. Local substrate temperature was measured using an external thermocouple attached to the surface of the test coupon. The resulting

Downloaded from http://meridian.allenpress.com/jmep/article-pdf/10/4/129/2244967/imaps_386.pdf by guest on 31 October 2022

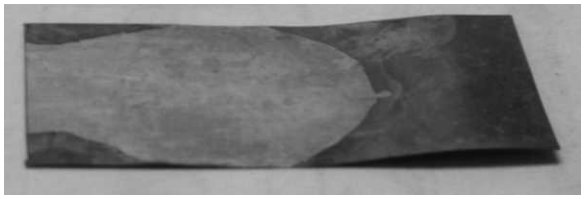

Fig. 6. As reflow sample of synthesized Sn-nanoparticle paste on top of a Cu substrate.

coupon exhibited a tinned surface where good wetting of the surface was observed as depicted in Fig. 6. SEM and EDS (Jeol JSM 6360 with EDS) was used to characterize the surface of the copper coupons.

SEM images in Fig. 7 show the surfaces obtained after the low temperature reflow process. EDS confirmed the presence of Sn over the Cu substrate as shown in Fig. 8. Reflow temperatures were approximately 30-40°C below the melting point of tin, therefore, in principle it has been demonstrated that using nanoparticles, the processing temperature of such a paste can be substantially reduced. However, due to the large amount of flux relative to metal within the paste, it was not possible to obtain enough volume of metal within the coupon, thus limiting the ability to form a solder joint as a device attach on an SMT process. The organic surfactant also played a critical role since it acted against the coagulation mechanisms needed for the surface melting required for the process. It has been theorized that increasing the metal load to 80 wt.% or more should eliminate this limitation, but the current flux/nanoparticle material cannot be mixed in such a high metal content ratio without affecting the necessary printability needed on a solder paste. In response to this observation, commercially procured Sn nanoparticles, without capping agent, were used for the formulation of a higher metal content Sn-nanoparticle paste.

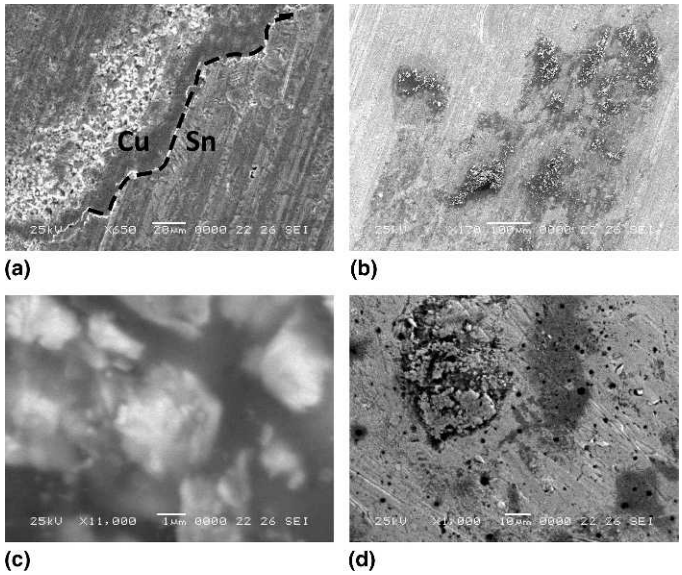

Fig. 7. SEM images of the surface of test coupons; (a) 205°C-interface copper-tin (tin on the right); (b) 205°C-surface defects; (c) 205°C-surface defects at x11 K; (d) 217°C-solder bump surface.

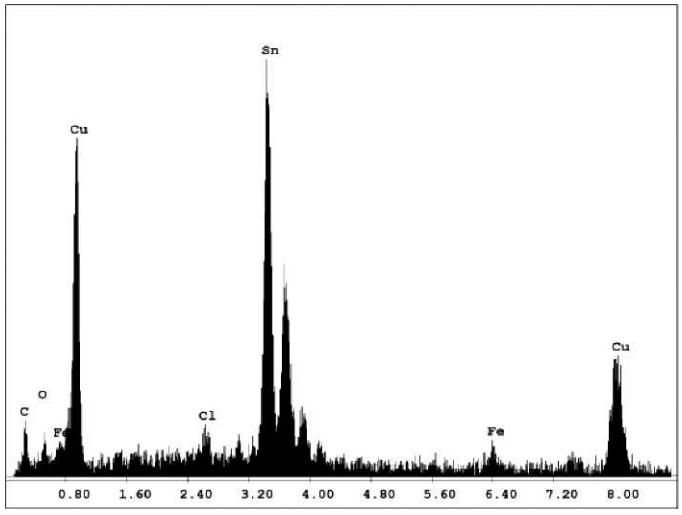

Fig. 8. EDS spectrum for the area shown in Fig. 7d.

B. Commercial Sn Nanoparticle Solder Paste

Commercially available Sn nanoparticles were procured from SSnano Inc. The nanoparticles specifications are: 99.9% of purity, an average particle size below 100 nm, spherical particles without surfactant, and a specific surface area of approximately 7 m^2/g. Fig. 9 shows an SEM image from the commercial nanoparticles. It can be observed that the particles are spherical and that, mostly, they are about 100 nm in diameter.

In order to avoid oxidation during the sintering process, flux containing 50 wt.% of ethylene glycol and 50 wt.% of glutamic acid was used to prepare the solder paste. After some experimental trials, the best embodiment for the paste was found to be 60 wt.% Sn nanoparticles and 40 wt.% flux.

Fig. 10 shows the reflow profiles used to process the samples, temperature was measured on top of the Cu foil substrate with an external thermocouple. The samples reached steady state temperature after 2 min. When using 180°C for processing, the samples did not hold up to the cleaning process of sonication in ethanol or acetone, thus this processing temperature was ruled out for all testing.

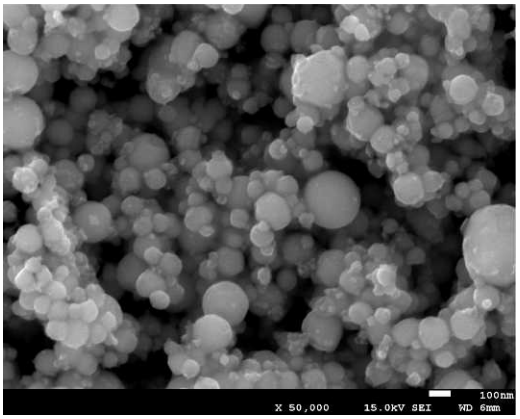

Fig. 9. SEM images of the Sn nanoparticles.

Downloaded from http://meridian.allenpress.com/jmep/article-pdf/10/4/129/2244967/imaps_386.pdf by guest on 31 October 2022

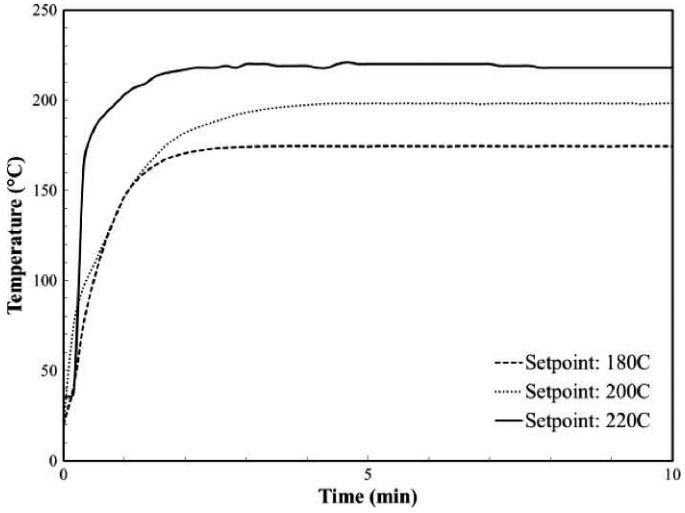

Fig. 10. Reflow profiles measured at the surface of the samples.

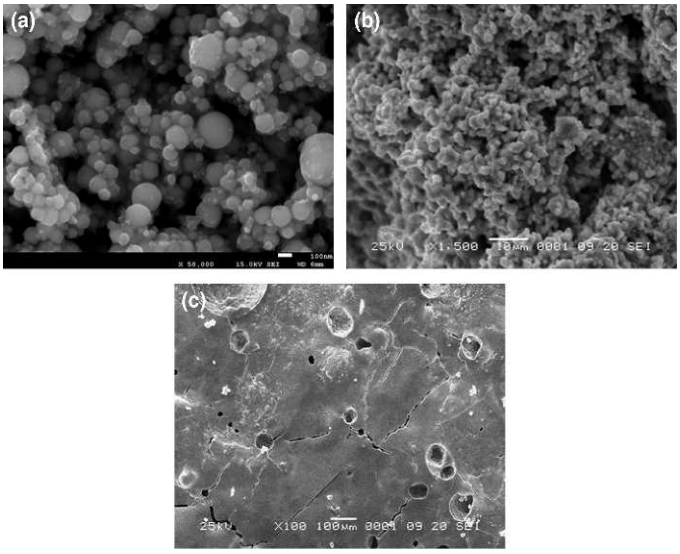

Fig. 11. SEM images confirming the sintering process at a temperature of 200°C; (a) loose nanoparticles; (b) 10 min; (c) 20 min.

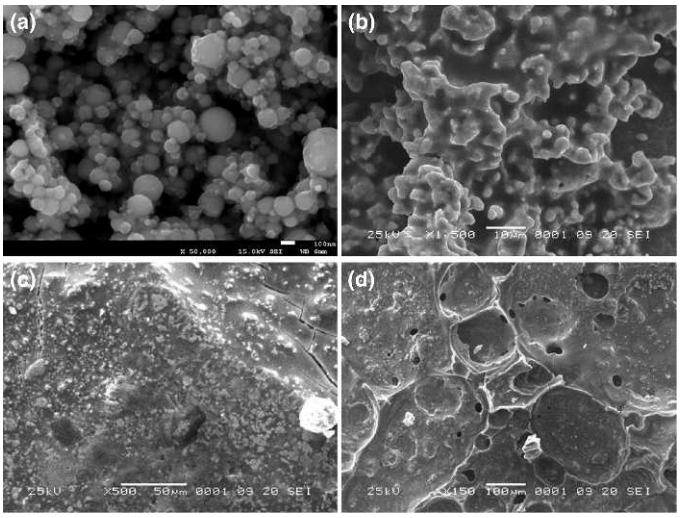

Fig. 12. SEM images confirming the sintering process at a temperature of 220°C; (a) loose nanoparticles; (b) 5 min; (c) 10 min; (d) 20 min.

For simplicity, solid-state densification is considered to be accomplished through three stages: initial, intermediate, and final. Multiple mechanisms are involved throughout these stages, namely, evaporation-condensation, surface diffusion, grain boundary diffusion, bulk diffusion, viscous flow, and plastic deformation [11]. In the initial stage, there is a growth of an interparticle neck. For nanoparticles, with excessive surface area and highly curved surfaces, surface diffusion is expected to be extremely rapid in this early sintering stage. Evidence of the surface diffusion contribution to the neck formation in nanopowder sintering has been given by many researchers [11]. During the intermediate and final stages, there is a substantial reduction in the pores and the interconnections increase with time, and at the final stage, grain growth is evident. Surface diffusion mechanisms are most sensitive to particle size. Therefore, enhanced surface diffusion with reduced low-temperature densification should be observed in sintering nanoparticles [11].

Fig. 11 and Fig. 12 show the evolution in the coalescence of nanoparticles at different temperatures, 200°C and 220°C, respectively. An initial attempt for the metallographic analysis using traditional techniques such as cross-sectioning and grinding/polishing resulted in exaggerated sintered features that were identified as artifacts of the metallography. Therefore, we proceeded with noninvasive metallographic techniques (e.g., surface imaging) to reveal the real as-fabricated features.

The first image in each figure (a) shows the loose Sn nanoparticles powder. Fig. 11 shows SEM images for a processing time of, for Fig 11(b), 10 min; and for Fig. 11(c), 20 min. Fig. 12 has images for Fig 12(b) of 5 min, for Fig. 12(c) of 10 min, and for Fig. 12(d), 20 min. At 200°C, the sample processed for 5 min did not withstand the cleaning process (5 min of sonication in acetone) and it can be inferred that the resulting structure at that time and temperature was not strong enough. The resulting structure improves as the processing time is longer. Also, by increasing the processing temperature, an improved structure could be obtained at a lower processing time. By visually inspecting Fig. 11(c) and Fig. 12(c), a similar surface structure was obtained at different conditions. The densification of the material highly depended on the processing time and temperature, an evident sintering mechanism of coalescence. From this morphological analysis, in addition to our goal to reduce the processing temperature, it was found that the samples processed at 200°C for 10 min appear to be superior to the other tested conditions. Necks between particles can also be observed in Fig. 11(b) and Fig. 12(b). Typical sintering behavior was observed by analyzing the resulting material surface and comparing the obtained results with published data on the sintering process of tungsten powder as shown in Fig. 13 where the similarities with our samples can be appreciated. The stages of sintering are shown at different times and temperatures. Fig. 11(b) shows the initial stage, Fig. 12(b) shows the intermediate stage, and Fig. 11(c) shows the final stage with significant grain growth and the typical pores for a sintered material.

Downloaded from http://meridian.allenpress.com/jmep/article-pdf/10/4/129/2244967/imaps_386.pdf by guest on 31 October 2022

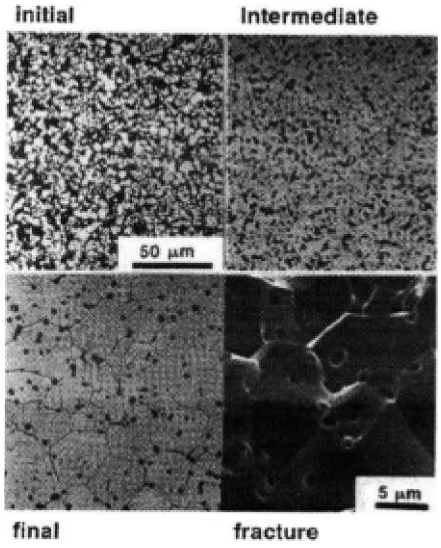

Fig. 13. Example of sintering progress in tungsten powder [10].

Using a GF-B-HT DDM Novastar reflow oven, the effect of argon during the process was assessed. The 200°C thermal profile was used to process the samples with and without argon for 20 min. For the samples processed in argon, a flow of 50 scfm was used with an oven purge time of 20 min.

SEM imaging was used to characterize the resulting surface for each case. Fig. 14(A) shows the typical surface obtained for the samples processed without argon and Fig. 14(B) shows the surface of the samples processed in argon. The samples processed with argon showed a less defective surface.

Using EDS analysis, the tin surface was analyzed in order to measure contaminants levels. Table I shows the average measurements for different samples. There is no significant difference between the samples processed with or without argon. No significant difference can be seen between the oxidation (O) levels of the samples. Also, high levels of chlorine (Cl) in both samples were found due to the flux acid.

Lap shear tests were performed in order to characterize the mechanical strength of the joints. An attempt to correlate the microstructure of the resulting attach material to the mechanical response was performed.

At 10 min, the sintering process began forming necks between adjacent nanoparticles resulting in a stronger structure than the 5 min sample that did not hold up. At the 20 min mark, the final stage of the sintering process was reached, as evidenced by the formation of a microstructure that resembles a bulk material, although still showing some porosity, which is intrinsic to the sintering process. After this point, the samples started to oxidize as time was increased, because no more flux was available to protect the metal. At 30 min, the structure showed some pitting corrosion, but in general the structure is similar, exhibiting pores and grain boundaries. Table II summarizes the quantity of oxygen at each stage found in the surfaces by using EDS. As shown in Fig. 15, at 200°C, the shear strength varied from 1.03 MPa to a maximum of 1.21 MPa for the sample processed at 20 min. Shear strength values for the eutectic Sn-Pb alloy ranging from 9.2 to 50 MPa have been published [17]. Common Pb-free solders, such as Sn-3.5Ag, Sn-0.7Cu, Sn-3.8Ag-0.7Cu, and Sn-3.5Ag-3Bi (by weight), have shown values ranging from 9.2 to 49 MPa [17]. Comparing the shear strength values, it can be seen that the mechanical properties of the developed nanosolder are below the commonly used alloys. The pores in the material were not included in the shear strength calculation, which could add to the difference between the experimental and theoretical values. However, there are applications such as MEMS packaging that may not require high mechanical strengths, but that are sensitive to processing temperatures; for those temperature-sensitive packages, this low processing temperature paste could be a solution.

Similarly, reflow profiles with peak temperature of 220°C and processing times of 5, 10, 20, and 30 min were used. After 20 min, the incremental oxidation of the samples became evident from the inspection. Processing times longer than 10 min are known to be detrimental for flux, where activators are basically consumed and no longer capable of providing any reducing or protecting function. Table II shows the oxygen weight percentage for each case, contrasting with the observations on SEM images. As time and temperature increases, the oxidation level increases. As seen from the mechanical data, the shear strength varied from 1.2-1.27 MPa, which is not a very significant change; however, its deterioration with time could be attributed to the higher oxidation rates (at 220°C the oxidation process started earlier because of the higher temperature).

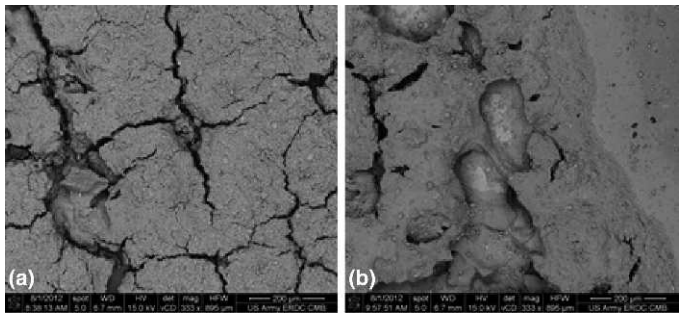

Fig. 14. SEM image of the tin surface after reflow in (a) ambient atmosphere (b) inert atmosphere (argon).

Table I
EDS Average Results for Different Samples and Areas

	EDS analysis average wt.% values	
	No argon	Argon
Sn	77.33	76.69
O	15.98	14.88
Cl	6.69	8.43

Table II
EDS Measurements on Oxygen Quantities

200°C		220°C	
Time (min)	O wt.%	Time (min)	O wt.%
		5	0.57
10	0.78	10	2.31
20	1.93	20	3.02
30	1.97	30	3.5

Downloaded from http://meridian.allenpress.com/jmep/article-pdf/10/4/129/2244967/imaps_386.pdf by guest on 31 October 2022

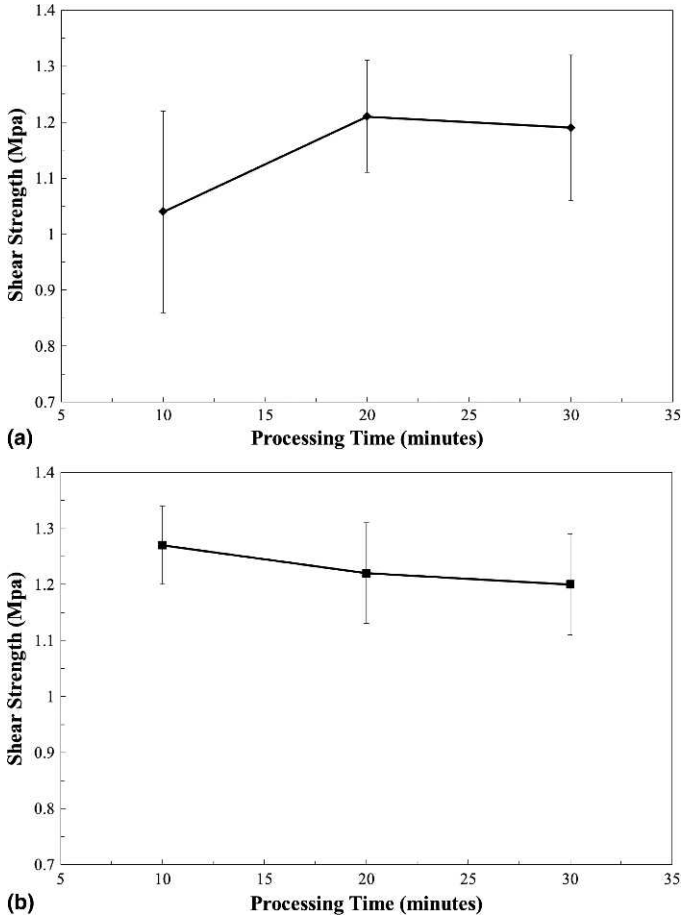

Fig. 15. Shear strength at different temperatures and times: (a) 200°C (b) 220°C.

The electrical conductivity of the sintered tin nanoparticles was measured and compared with the bulk value reported in the literature [18].

The resulting averaged conductivity values and the theoretical value for tin are shown in Table III. Both measured values were several orders of magnitude below the theoretical value. The conductivity of the sintered material gets a slight increase by the use of argon. As shown in Fig. 14, an improvement of the surface is acquired when the samples are processed under an argon atmosphere. The difference between the experimental and theoretical values can be attributed to the porous structure obtained via sintering. The cross-sectional area used in the resistivity calculations does not take into account the pores of the structure.

Table III
Average Electrical Conductivity Values

	Experimental, no argon	Experimental, argon	Theoretical [18]
Electrical conductivity (S/m)	1.36×10^5	3.29×10^5	910.6×10^6

C. Thermal Characterization

The DSC curve obtained for the 1,10 phenanthroline-capped tin nanoparticles, shown in Fig. 16, exhibited the thermal characteristics of this material. A transformation at ∼111°C was observed and attributed to the melting of the 1,10 phenanthroline (the nanoparticles' capping agent); this behavior showed some difference when compared with the isolated capping agent. The bond of the capping agent with the nanoparticle is different from the bond with itself. From previous analysis on the isolated 1,10 phenanthroline, it was observed that it completely evaporates below 200°C. Using off-line thermogravimetry, a quantitative estimation of the capping agent of the nanoparticles was performed. It was determined that approximately 20% of the weight of the synthesized nanoparticles is 1,10 phenanthroline. The second transformation occurs at about 228°C which is attributed to the melting of tin. A DSC profile (depicted in Fig. 16) for bulk tin served as a comparative basis for the nanomaterials. According to the data, the synthesized tin nanoparticles showed a depression of 4°C in their melting point, where 232°C is the melting point measured for bulk tin. The as-received commercial nanoparticles were characterized using the DSC, Fig. 16 shows the pattern for the sample. The profile shows an endothermic peak related

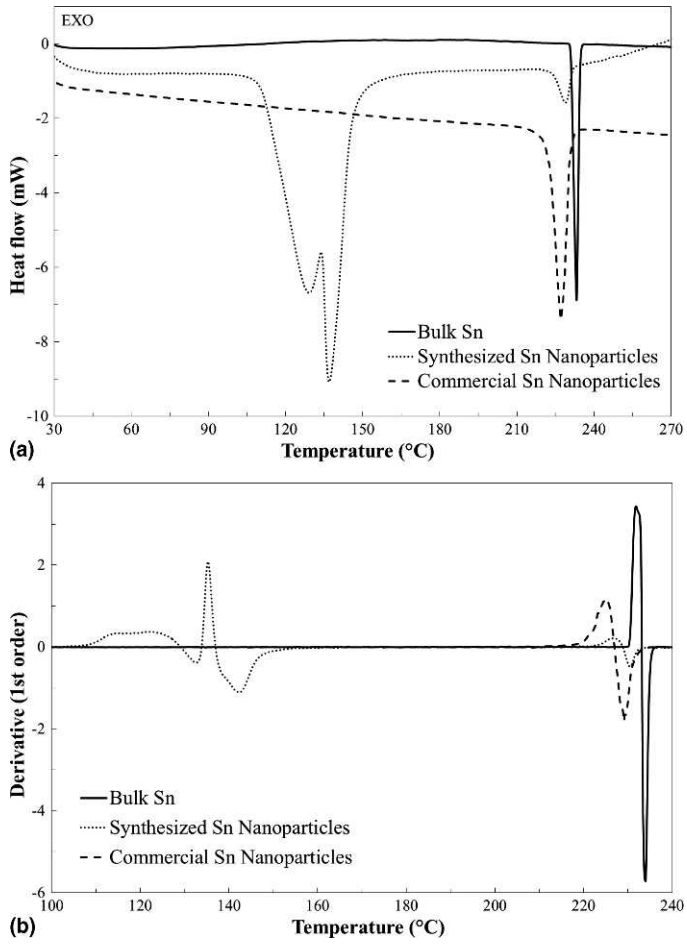

Fig. 16. Thermal analysis for the metallic materials: (a) DSC profiles (b) first derivative.

Downloaded from http://meridian.allenpress.com/jmep/article-pdf/10/4/129/2244967/imaps_386.pdf by guest on 31 October 2022

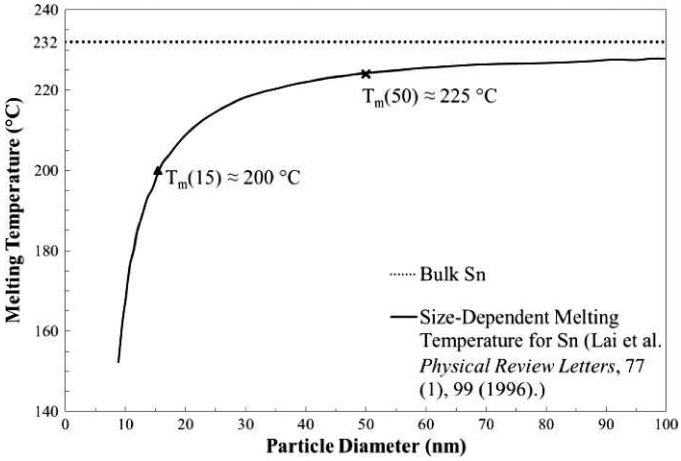

Fig. 17. Tin melting point depression curve as function of particle size.

to the melting of the nanoparticles. The melting process occurs around 227°C. Commercial nanoparticles have shown a melting point depression of about 5°C.

The flux was analyzed using different DSC thermal profiles. With a ramp profile up to 300°C, the weight loss due to evaporation of the constituents was around 68%. Using a ramp and isothermal hold temperature at 200°C for 20 min (profile similar to the optimal processing condition used), the weight loss was around 62%, which suggests that the samples after reflow have ∼38% by weight of residues from the flux. The effect of the ramp steepness (heating rate) was assessed using two different ramps with the same holding time. The steeper ramp, 60°C/min, produced the best surface on the solder (less roughness). As stated by Groza [11], the consolidation mechanism works better when high ramps are used.

Fig. 17 shows the melting point depression curve for tin as function of particle radius. Assuming that the onset of the DSC curve was approximately 225°C for both nanomaterials, that is, synthesized and procured nanoparticles, the following analysis was performed. Using a melting point temperature of 225°C, the average diameter of the nanoparticle should be 50 nm according to melting point depression curve. The optimal experimental processing temperature used was 200°C. From inspection, a particle diameter of ∼15 nm is required if melting at 200°C is expected. The average particle diameter for the synthesized nanoparticles was approximately 45 nm and 94.6 nm for the commercially procured nanoparticles. The commercial nanoparticles have a better match with the theoretical value for melting point depression; however, the synthesized nanoparticles are off by approximately 5°C. The synthesized nanoparticles have around 20% by weight of the capping agent; this could be the causal factor for the incongruity between the theoretical and experimental results. A critical observation is that coalescence of the nanoparticles was attained at 200°C, thus proving that if the nanoparticles are not small enough, the mechanism that dominates is sintering where mass transfer between particles promotes the formation of a continuous body. Below a radius of 10 nm, the depression curve gets steeper; therefore, in this region the melting point depression should dominate the coalescence process.

Conclusion

Sn nanoparticles were successfully synthesized and used in the formulation of a novel, proof-of-concept nanosolder paste. Low temperatures conditions (∼200°C), well below those needed for SAC Pb-free reflow, were used to process the nanosolder paste, which resulted in the successful formation of a tinned copper substrate. However, owing to the low metal content and the presence of the organic surfactant, the formation of a bulk metallic joint was not possible at this stage.

Commercially available Sn nanoparticles, with no capping agent, were used to prepare a solder paste with higher metallic content in order to prove the concept developed from our synthesized paste. After a series of experimental trials, a successful nanopaste was obtained with a best embodiment of 60 wt.% Sn nanoparticles and 40 wt.% flux. From qualitative tests, this paste proved to be a potential solution for the reduction of processing temperature on Pb-free solders. Microstructural analysis and mechanical testing were used to characterize the joints, which were further related to the process parameters. The suggested condition, when processing the sample in air, was defined to be 20 min at 200°C, which resulted in an evolved metallic microstructure with minimal pores, peak mechanical response, and the lowest processing temperature. Prolonged processing times and higher temperatures resulted in excessive oxidation due to the loss of flux presence.

From thermal analysis of the materials, the nanoparticles showed a melting point depression of 5°C. The mechanism that ruled the coalescence of the nanoparticles was sintering. The critical parameters in the processing of the samples were time and temperature. With longer times and higher temperatures, the oxidation process of the samples was accelerated. Also, the thermal analysis showed that the capping agent on the synthesized nanoparticles accounts for 20% of the total weight. The analysis from the solder paste showed that a considerable amount of residue from the flux remained in the final material.

Although it is well known that pure Sn solders have a tendency to grow whiskers, in this work we have demonstrated the use of Sn nanoparticles to develop a solder paste that will serve as the basis for the future development of a nano-Sn rich alloy for device interconnects.

Acknowledgments

This work was sponsored by a Lockheed Martin Corporation (LMC) University Research Agreement. The authors thank Dr. Wilfredo Otaño from UPR-Cayey for his support by lending his laboratory and equipment for the characterization work.

References

[1] C. Kazmierski, "Semiconductor Industry Association: Semiconductor year-over-year sales growth encouraging," Available at http://www.sia-online.org/news/2011/05/31/global-sales-reports-2011/semiconductor-year-over-year-sales-growth-encouraging/ Retrieved April 30, 2012, 2011.

[2] J. Illyefalvi-Vitez, Z. Krammer, and O. Pinkola, "Testing the impact of Pb-free soldering on reliability," *Electronics Systemintegration Technology Conference*, Vol. 1, pp. 468-473, 2006.

[3] C.D. Zou, Y.L. Gao, B. Yang, X.Z. Xia, Q.J. Zhai, C. Andersson, and J. Liu, "Nanoparticles of the lead-free solder alloy Sn-3.0Ag-0.5Cu with large melting temperature depression," *Journal of Electronic Materials*, Vol. 38, No. 2, pp. 351-355, 2008.

Downloaded from http://meridian.allenpress.com/jmep/article-pdf/10/4/129/2244967/imaps_386.pdf by guest on 31 October 2022

[4] J.E. Morris, "Nanoparticles properties," in *Nanopackaging: Nanotechnologies and Electronics Packaging*, Springer, Berlin, pp. 93-107, 2008.
[5] S. Lai, J. Guo, V. Petrova, G. Ramanath, and L. Allen, "Size-dependent melting properties of small tin particles: Nanocalorimetric measurements," *Physical Review Letters*, Vol. 77, No. 1, pp. 99-102, 1996.
[6] C. Zou, Y. Gao, B. Yang, and Q. Zhai, "Size-dependent melting properties of Sn nanoparticles by chemical reduction synthesis," *Transactions of Nonferrous Metals Society of China*, Vol. 20, No. 2, pp. 248-253, 2010.
[7] V.V. Lubashenko, "Size-dependent melting of nanocrystals: A self-consistent statistical approach," *Journal of Nanoparticle Research*, Vol. 12, No. 5, pp. 1837-1844, 2009.
[8] H. Jiang, K.J. Moon, and C. Wong, "Nanolead-free solder pastes for low processing temperature interconnect applications in microelectronic packaging," *Nano-Bio-Electronic, Photonic and MEMS Packaging*, p. 217, 2009.
[9] K. Nanda, "Size-dependent melting of nanoparticles: Hundred years of thermodynamic model," Pramana, Vol. 72, No. 4, pp. 617-628, 2009.
[10] U. Olevsky and A. Eugene, "Sintering theory: A brief introduction," *Presentation at Technische Universität Darmstadt*, 2011.
[11] J.R. Groza, "Nanocrystalline powder consolidation methods," *Nanostructured Materials: Processing, Properties and Applications*, pp. 115-178, 2007.
[12] H. Jiang and C.P. Wong, "Low processing temperature of lead-free solder interconnects," *IEEE Nanotechnology Magazine*, Vol. 4, No. 2, pp. 20-23, 2010.
[13] M. Schmidt, R. Kusche, and H. Haberland, "Irregular variations in the melting point of size-selected atomic clusters," *Nature*, Vol. 393, No. May, pp. 238-240, 1998.
[14] H. Jiang, K. Moon, F. Hua, and C.P. Wong, "Synthesis and thermal and wetting properties of tin/silver alloy nanoparticles for low melting point lead-free solders," *Chemistry of Materials*, Vol. 19, No. 18, pp. 4482-4485, 2007.
[15] L.-Y. Hsiao and J.-G. Duh, "Synthesis and characterization of lead-free solders with Sn-3.5Ag-xCu (x= 0.2, 0.5, 1.0) alloy nanoparticles by the chemical reduction method," *Journal of the Electrochemical Society*, Vol. 152, No. 9, p. J105, 2005.
[16] J. Liu, C. Andersson, Y. Gao, and Q. Zhai, "Recent development of nano-solder paste for electronics interconnect applications," Proceedings of the 10th Electronics Packaging Technology Conference, EPTC 2008, pp. 84-93, 2008.
[17] S.K. Kang, "Recent progress in lead (Pb)-free solders and soldering technology," *Workshop on Pb-Free Solders, UCLA*, 2002.
[18] M. Karamargin and C. Reynolds, "Thermal and electrical conductivity of pure tin from 4.5 to 77° K," *Physical Review B: Condensed Matter and Materials Physics*, Vol. 5, pp. 2856-2863, 1972.

Downloaded from http://meridian.allenpress.com/jmep/article-pdf/10/4/129/2244967/imaps_386.pdf by guest on 31 October 2022